electronics

MDPI

Article

Detection of Ventricular Fibrillation Using Ensemble Empirical Mode Decomposition of ECG Signals

Seungrok Oh and Young-Seok Choi *

Department of Electronics and Communications Engineering, Kwangwoon University, Seoul 01897, Republic of Korea
* Correspondence: yschoil@kw.ac.kr

Abstract: Ventricular fibrillation (VF) is a critical ventricular arrhythmia with severe consequences. Due to the severity of VF, it urgently requires a rapid and accurate detection of abnormal patterns in ECG signals. Here, we present an efficient method to detect abnormal electrocardiogram (ECG) signals associated with VF by measuring orthogonality between intrinsic mode functions (IMFs) derived from a data-driven decomposition method, namely, ensemble empirical mode decomposition (EEMD). The proposed method incorporates the decomposition of the ECG signal into its IMFs using EEMD, followed by the computation of the angles between subsequent IMFs, especially low-order IMFs, as the features to discriminate normal and abnormal ECG patterns. The proposed method was validated through experiments using a public MIT-BIH ECG dataset for its effectiveness in detecting VF ECG signals compared to conventional methods. The proposed method achieves a sensitivity of 99.22%, a specificity of 99.37%, and an accuracy of 99.28% with a 3 s ECG window and a support vector machine (SVM) with a linear kernel, which performs better than existing VF detection methods. The capability of the proposed method can provide a perspective approach for the real-time and practical computer-aided diagnosis of VF.

Keywords: electrocardiogram (ECG); ventricular fibrillation (VF); ensemble empirical mode decomposition (EEMD); intrinsic mode function (IMF); orthogonality

Citation: Oh, S.; Choi, Y.-S. Detection of Ventricular Fibrillation Using Ensemble Empirical Mode Decomposition of ECG Signals. *Electronics* **2024**, *13*, 695. https://doi.org/10.3390/electronics13040695

Academic Editors: Enzo Pasquale Scilingo and Gabriella Olmo

Received: 9 December 2023
Revised: 4 February 2024
Accepted: 6 February 2024
Published: 8 February 2024

1. Introduction

The electrocardiogram (ECG) is a crucial diagnostic tool that measures and records the electrical activity of the heart. An ECG is typically measured using electrodes on the chest, arms, and legs [1,2]. ECG signals can be easily measured and thus are a helpful non-invasive tool. Due to its simplicity, ECG signals are widely considered in various biomedical applications, such as heart rate variability (HRV), diagnosing heart deformity, emotion recognition, biometric identification, and so forth [3–6].

Of particular significance in the analysis of ECG signals is the diagnosis of cardiac arrhythmias and life-threatening heart conditions. According to recent studies in [7,8], cardiac arrhythmias are the most common reason for cardiovascular disease death. Therefore, the accurate detection of cardiac arrhythmias has been of great interest in ECG analysis. Ventricular fibrillation (VF) is the leading cause of sudden cardiac arrest, making it a cardiac arrhythmia that threatens life [9]. VF's hallmark is its obscured QRST complex in ECG traces and volatile and unpredictable signal deflections, rendering the rhythm chaotic [10]. Moreover, the deflections in ECG signals continuously change in shape, magnitude, and direction. Patients experiencing VF require a high-amplitude current impulse to the heart to restore normal rhythm. Defibrillation is typically achieved by a 200 J shock applied externally to the chest or a 20 J shock applied internally to the heart [11]. To deliver shocks or interventions, abnormal ECG rhythms must be detected rapidly and correctly. In this situation, two issues are considered: (1) a false positive (FP) occurs; for example, if a normal sinus rhythm (NSR) is misdiagnosed as VF, it produces an unnecessary shock on the heart,

which can damage the heart of the patient. (2) if a patient experiencing VF is left without taking adequate treatment, it causes cardiac arrest and sudden cardiac death. Therefore, the reliable detection of VF using short-term ECG signals is a crucial issue for saving lives in practical situations.

Over the decades, a number of signal-processing methods for detecting abnormal ECG signals have been developed. Among them, frequency-domain methods such as Hilbert transform [12,13], Fourier transform [14,15], subband decomposition [16], and power spectral density [17] have been developed. Time-frequency domain approaches have gained popularity when considering the non-stationarity property of ECG signals [9,18,19]. In addition, wavelet transform has been considered in analyzing ECG signals [20–22]. However, since the aforementioned methods use predefined basis functions, they suffer from reflecting inherently nonlinear characteristics of ECG signals [23].

More recently, advanced machine-learning and deep-learning models in ECG analysis have been actively researched [24,25]. The use of deep learning might address the labor-intensive issue of the handcrafted feature-extraction-based ECG analysis.

To address the fixed basis function issue for a decomposing signal, a data-driven method, known as empirical mode decomposition (EMD), has been developed [26]. EMD is an adaptive method for analyzing nonstationary signals; thus, it is adequate and used for analyzing ECG signals [27–29]. It produces a sum of amplitude and frequency-modulated functions, namely, intrinsic mode functions (IMFs). EMD has been known as a suitable tool for analyzing nonlinear and nonstationary signals regardless of the length of the signals. In [30], using EMD in detecting abnormal ECG signals has led to an improved detection of VF. Despite its potential, EMD is not without flaws, primarily due to a phenomenon known as mode mixing, which causes nonphysical IMFs.

To address a mode mixing issue, ensemble empirical mode decomposition (EEMD) has been presented by employing decomposition over a set of noisy signal versions and following an averaging [31]. In recent studies, EEMD has been used to analyze biological signals such as ECG [32–34]. Although the EEMD technique has been previously used to analyze ECG signals, most works have focused on denoising ECG signals [35,36]. No work has been presented to detect abnormal VF from ECG signals using orthogonality between IMFs.

Motivated by the properties of the narrowband components of the EMD of ECG signals [30,37,38], we present a new VF detection method that consists of EEMD and orthogonality analysis of IMFs with short-term ECG signals. EEMD is used to decompose an ECG signal into its IMFs. Then, we compute the degree of orthogonality between consecutive IMFs as features to distinguish VF ECG patterns.

The ECG signals of the NSR and VF ECG signals are shown in Figure 1. As shown in Figure 1, NSR, as a standard ECG signal, exhibits clear QRS complexes, thus producing subsequent IMFs, i.e., narrowband components, with nonorthogonality. On the contrary, since QRS complexes lack VF ECG signals, they produce orthogonal IMFs. This observation forms the basis of our approach, where we use angles between specific IMFs, especially two angles between the first and second IMFs and the second and third IMFs, as features for a linear kernel support vector machine (SVM). The efficacy of our method has been tested using a recognized MIT-BIH arrhythmia database [39], and the results, benchmarked against traditional techniques, highlight its potential.

The rest of the paper is organized as follows: In Section 2, we introduce EMD, EEMD, and the feature selection of the proposed method. In Section 3, the experimental results are provided. Section 4 provides the discussion, and Section 5 concludes this work.

NSR - Normal Sinus Rhythm

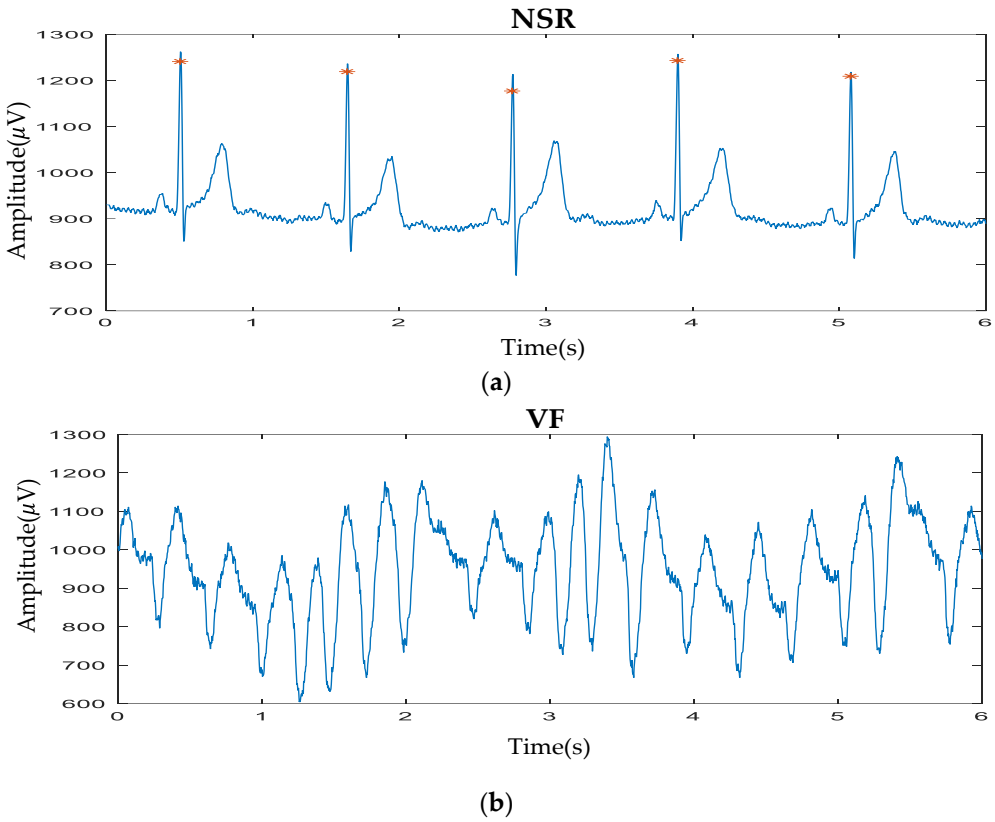

Figure 1. Typical ECG waveforms of NSR and VF cases. The red stars denote R-peaks: (**a**) a typical NSR ECG waveform of NSR; (**b**) a typical VF ECG waveform.

2. Materials and Methods

This section describes the proposed method to discriminate VF ECG signals from NSR ECG ones.

2.1. Empirical Mode Decomposition

Huang et al. [26] have developed a data-driven decomposition method suited for analyzing nonlinear and nonstationary signals. Iteratively termed a sifting process, EMD extracts the highest frequency oscillation (most fine temporal scale) from the signal, called an IMF. The remaining part, after extraction, contains lower-frequency oscillatory components. The resulting IMFs represent the oscillatory patterns at different frequency scales. It gives rise to the significant feature of EMD: EMD results in basis functions derived from the signal in a self-originated way, whereas other conventional methods, such as Fourier and wavelet analyses, rely on predefined basis functions.

An IMF must meet the following two criteria: (1) the number of extreme and zero crossings are either equal or differ by at most one, and (2) the mean value of the envelope defined by the local maxima and local minima is zero.

Here, we describe the process of EMD as follows. For a given signal $x(t)$, the process of EMD consists of the following steps:

(1) Identify all local maxima and minima of $x(t)$. Let $i, j = 1$;
(2) Interpolate between local maxima and minima, respectively, obtaining an upper envelope $e_u(t)$ and a lower envelope $e_l(t)$;
(3) Compute the mean between $e_u(t)$ and $e_l(t)$, i.e., $m_{i,j}(t) = \frac{[e_u(t)+e_l(t)]}{2}$;
(4) Extract the detail from the original signal as $d(t) = x(t) - m_{i,j}(t)$;
(5) Iterate steps (1)–(4) until $d(t)$ satisfies the above two criteria to be an IMF, i.e., $c_1(t) = d(t)$. If not, increase j by 1;
(6) Compute the residue $r_1(t) = x(t) - c_1(t)$;

(7) Iterate through Steps (1)–(6) with $r_1(t)$ instead of $x(t)$ until the residue satisfies some stopping criterion. Also, increase i by 1.

Figure 2 shows a sifting process of a real NSR ECG signal. It demonstrated a mean envelope originated from an upper envelope and a lower envelope of raw ECG signals.

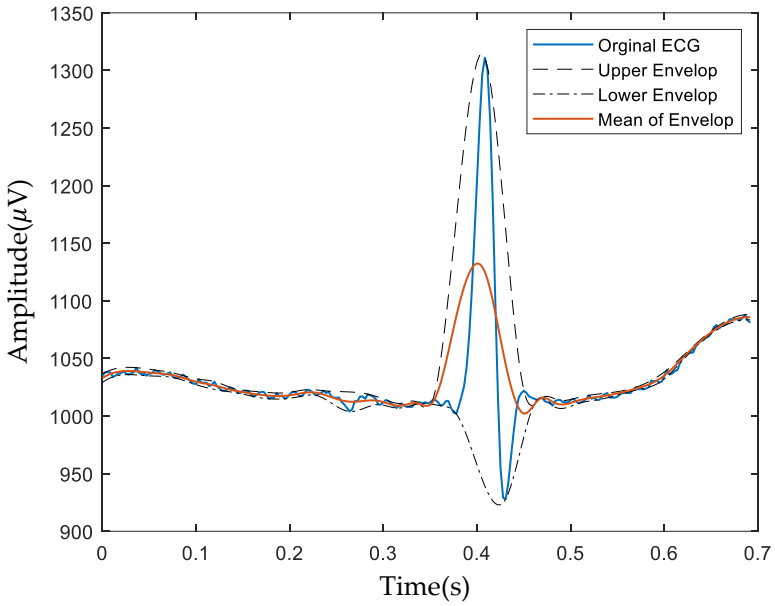

Figure 2. Sifting process of the ECG signal.

Whether a sifting process is stopped or not, the standard deviation computed from two consecutive sifting processes is used [26].

Through the EMD sifting process of EMD, the signal $x(t)$ is decomposed as follows:

$$x(t) = \sum_{i=1}^{M} c_i(t) + r_M(t) \tag{1}$$

where M is the number of all extracted IMFs, $c_i(t)$, $i = 1, \ldots, M$ denotes the IMFs, and $r_M(t)$ is the final residue. The last residue can be considered as the last IMF, and thus Equation (1) can be rewritten as $x(t) = \sum_{i=1}^{M+1} c_i(t)$.

Despite several advantages of EMD, it suffers from a mode mixing issue. Mode mixing indicates the possibility that distinct IMFs may exhibit similar frequency components. This matter raises the intangible importance of IMFs.

2.2. Ensemble Empirical Mode Decomposition

EEMD has been developed to address the mode mixing problem inherent in EMD [31]. It uses a noise-added data analysis approach. EEMD consists of a sifting process of an ensemble of white noise-added signals and defining the true IMFs of a signal as the mean of an ensemble of trials.

For EEMD, to yield an ensemble of noise-added signal $x_v(t)$, the white Gaussian noise (WGN) $v(t)$ is perturbed to yield the signal $x(t)$, i.e., $x_v(t) = x(t) + v(t)$. Subsequently, the EMD algorithm is carried out to yield the ensemble signal $x_v(t)$. This procedure is carried out repeatedly.

This is performed for the different L realizations of WGN. The actual IMFs of EEMD are obtained by averaging the IMFs obtained from different realizations. The use of WGN leads to the ensemble of all solutions through the sifting process. In addition, due to the characteristic of the dyadic filter bank of EMD, the resulting IMFs of EEMD merge different scale components.

Specifically, the EEMD method is carried out as follows:

(1) Add WGN to the original signal $x_v(t) = x(t) + v(t)$;
(2) Apply the EMD method to $x_v(t)$ to obtain IMFs $c_i(t),\ i = 1, \ldots, M$;
(3) Repeat Steps (1) and (2) for L realizations of WGN. From the kth realization, the IMFs $c_i^k(t),\ i = 1, \ldots, M$ are obtained;
(4) Obtain an averaged IMFs $\bar{c}_i = \frac{1}{L}\sum_{k=1}^{L} c_i^k(t)$.

2.3. The Proposed VF Detection Using EEMD

We used the first three IMFs to discriminate NSR and VF using ECG signals. Although the QRS complex of the ECG signals spreads over the IMFs, the lower the order of the IMFs, the greater the QRS complex. As shown in Figures 3 and 4, as the order of IMFs increases, the lower frequency components of IMF are extracted. It is in accordance with the principle of EMD and EEMD in that they extract the highest frequency components of the signal of interest first, and then lower frequency components are extracted. Here, the first three IMFs from the EMD (Figure 3a,b) and from the EEMD (Figure 4a,b) of subjects with NSR and VF, respectively. Subjects were chosen randomly from the ECG database.

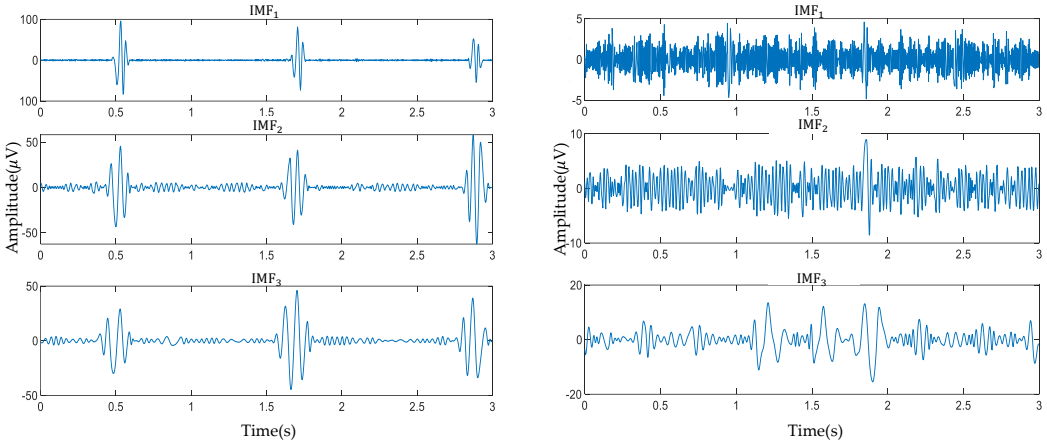

Figure 3. The first three IMFs (denoted as IMF_1, IMF_2, and IMF_3) after applying EMD to the MIT-BIH arrhythmia database: (**a**) First three IMFs in the case of Subject No. 117 (NSR); (**b**) First three IMFs in the case of Subject No. 418 (VF).

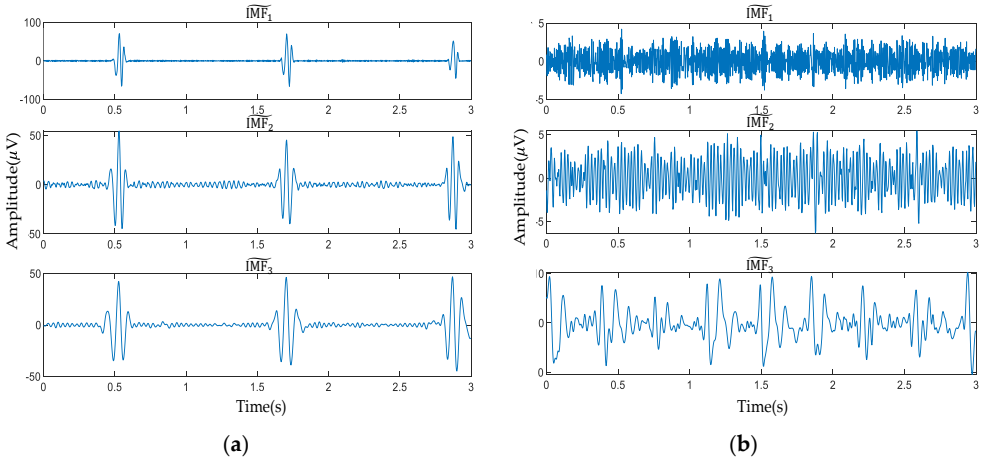

Figure 4. The first three IMFs (denoted as $\bar{c}_1$, $\bar{c}_2$, and $\bar{c}_3$) after applying EEMD to the MIT-BIH arrhythmia database: (**a**) First three IMFs in the case of Subject No. 117 (NSR); (**b**) First three IMFs in the case of Subject No. 418 (VF).

In other words, the components of the sharp QRS complex with high frequency are assigned to the lower-order IMF signal, so the impact of the QRS complex decreases as the order of the IMF increases [40]. In the NSR cases shown in Figures 3a and 4a, it has been observed that values outside the QRS complex are nearly zero. In contrast, in the case of VF in Figures 3b and 4b, the QRS complex in low-order IMFs appears to be absent.

Then, to validate the ability of NSR and VF to differentiate through analytics, we concentrate on the property that leaks the orthogonality of the IMFs of the NSR and VF episodes. The orthogonality is not guaranteed theoretically. All IMFs should be local orthogonal to each other because each component is obtained from the difference between the signal $x(t)$ and its local mean $\overline{x(t)}$ through the maximal and minimal envelopes [30,41,42]. Thus, in an ideal case, the following formula holds.

$$\overline{c_1(t)\cdot c_2(t)} = \overline{\left(x(t) - \overline{x(t)}\right)\cdot\overline{x(t)}} = \overline{\left(x(t)\cdot\overline{x(t)}\right)} - \overline{x(t)}\cdot\overline{x(t)} = 0, \quad (2)$$

where $c_1(t) = x(t) - \overline{x(t)}$ and $c_2 = \overline{x(t)}$. However, Equation (2) is not strictly true because the mean is calculated using the envelopes. The discrepancy between the envelope average and the actual local average for signals from nonlinear dynamic systems exists [43,44]. Moreover, each consecutive IMF component is only part of the signal constituting $\overline{x(t)}$. The first IMF is expressed as

$$c_1(t) = d_k(t) = d_{k-1}(t) - m_{1,k}(t) = d_{k-2}(t) - m_{1,\,k-1}(t) - m_{1,k}(t) \quad (3)$$

Here, $d_k(t)$ denotes a k-th detail, and $m_{i,j}(t)$ denotes the mean of the upper and lower envelopes in the j-th iteration for the i-th IMF.

Finally, it becomes

$$c_1(t) = x(t) - \sum_{i=1}^{k} m_{1,i}(t) \quad (4)$$

Followingly, $c_2(t)$ can be represented by replacing $x(t)$ with $r_1(t)$ and $m_{1,i}(t)$ with $m_{2,i}(t)$ in Equation (4) as

$$c_2(t) = r_1(t) - \sum_{i=0}^{k} m_{2,i}(t) \quad (5)$$

Then, the following holds:

$$c_2(t) = x(t) - c_1(t) - \sum_{i=0}^{k} m_{2,i}(t) = \sum_{i=0}^{k} m_{1,i}(t) - \sum_{j=0}^{l} m_{2,j}(t) \quad (6)$$

Then, it leads to

$$\overline{c_1(t)\cdot c_2(t)} = \overline{\left(x(t) - \sum_{i=0}^{k} m_{1,i}(t)\right)\cdot\left(\sum_{i=0}^{k} m_{1,i}(t) - \sum_{j=0}^{l} m_{2,j}(t)\right)} \quad (7)$$

The discrepancy between Equations (2) and (7) is due to an approximation that depends on the type of ECG signals. In this work, our observation reveals that the discrepancy of VF ECG signals is less evident than that of NSR ECG signals when the initial few IMFs, i.e., higher oscillatory components, are considered. Furthermore, our observations show that the leakage is greater when EEMD is applied for NSR ECGs compared to the case of EMD. On the other hand, the leakage is smaller when EEMD is used for VF ECGs than when EMD is used.

Thus, we utilize the features for discriminating VF from NSR by reflecting the property of orthogonality between consecutive initial IMFs, which is given by

$$< \mathrm{IMF}_1, \mathrm{IMF}_2 > = \|\mathrm{IMF}_1\|\|\mathrm{IMF}_2\|\cos\theta_{12} \quad (8)$$

$$< \mathrm{IMF}_2, \mathrm{IMF}_3 >= \|\mathrm{IMF}_2\| \|\mathrm{IMF}_3\| \cos\theta_{23} \quad (9)$$

where $\mathbf{IMF}_k$ is a k-th IMF vector, $< \cdot, \cdot >$ denotes an inner product, and θ_{ij} is an angle between the i-th and j-th IMFs.

Finally, the angles θ_{12} and θ_{23} are utilized as features for classifying VF from NSR, since the QRS complex is well reflected in the first three IMFs [40].

2.4. Real ECG Data

The Boston Israel Hospital and MIT (MIT-BIH) arrhythmia database [39] is used for the experiments. The MIT-BIH Arrhythmia Database comprises 48 half-hour excerpts from two-channel ambulatory ECG recordings. These were obtained from 47 subjects who were studied by the BIH Arrhythmia Laboratory. Each ECG recording consists of two channels and is recorded with a sampling rate of 360 Hz. All data we used were taken from channel II according to the cardiologist's annotations. Then, we divided the data into 3 s for the EMD and EEMD processes. Next, we arbitrarily selected 7338 episodes of 3 s in length for NSR and 6615 episodes for VF. We used a 3 s length for NSR and 6615 episodes for VF to detect the VF ECG signals using short-term recordings.

3. Results

To verify the proposed method, we used ECG signals with a 3 s length, which are used for the EMD and EEMD process.

First, we validate the features, i.e., θ_{12} and θ_{23}, in terms of their distributions. Figure 5 presents the histograms of the probability distribution for the angles θ_{12} and θ_{23} between the first three IMFs resulting from applying EMD and EEMD to ECG episodes characterized as NSR and VF. In Figure 5a, the EMD method is used, and it shows two histograms of θ_{12} and θ_{23} for each comparison of IMFs: one for NSR (pink) and one for VF (green), respectively. Each histogram is accompanied by a normal distribution fit, illustrating how the angles are distributed for NSR and VF episodes. It can be observed that for VF, the angles θ_{12} and θ_{23} tend to cluster around a narrower range as indicated by the sharper peak of the histogram, whereas for NSR, the angles are more spread out, resulting in a flatter histogram shape.

Figure 5b shows the histograms and the corresponding normal distribution fits of θ_{12} and θ_{23} for NSR and VF using EEMD. As can be seen, the angles for the θ_{12} and θ_{23} of VF are more concentrated around a mean value, whereas the angles of NSR are more dispersed. In addition, the values of θ_{12} and θ_{23} derived by EEMD are lower than those by EMD, especially for NSR. It suggests that using EEMD leads to a more discriminable capability between NSR and VF.

From Figure 5, we can observe that the angles θ_{12} and θ_{23} are larger in VF than in the NSR, and almost orthogonal (approximately 90°) in the case of VF. Although detection of VF from NSR might be available using only θ_{12} based on the histogram results, using θ_{23} can lead to accurate discrimination between NSR and VF. Overall, the histograms suggest that the angles between the first three IMFs from ECG signals exhibit different probability distributions in cases of NSR versus VF. Note that the angles between the three IMFs of VF show a tighter cluster, indicative of more regular and periodic behavior. At the same time, NSR displays a broader spread of angles, reflecting the more chaotic nature of the arrhythmic condition.

Figure 6 presents scatter plots for the angles, i.e., θ_{12} and θ_{23}, derived from EMD and EEMD when applied to the NSR and VF ECG recordings. Figure 6a depicts the scatter plot resulting from EMD. The plot shows the angle between the first two IMFs on the x-axis (θ_{12}) against the angle between the second and third IMFs on the y-axis (θ_{23}). Red circles represent NSR episodes, and blue circles denote VF episodes. The distribution of NSR points is more concentrated towards the lower end of the angle spectrum, indicating a more regular rhythmic pattern, while VF points are widely dispersed, reflecting the irregular and chaotic nature of the VF condition.

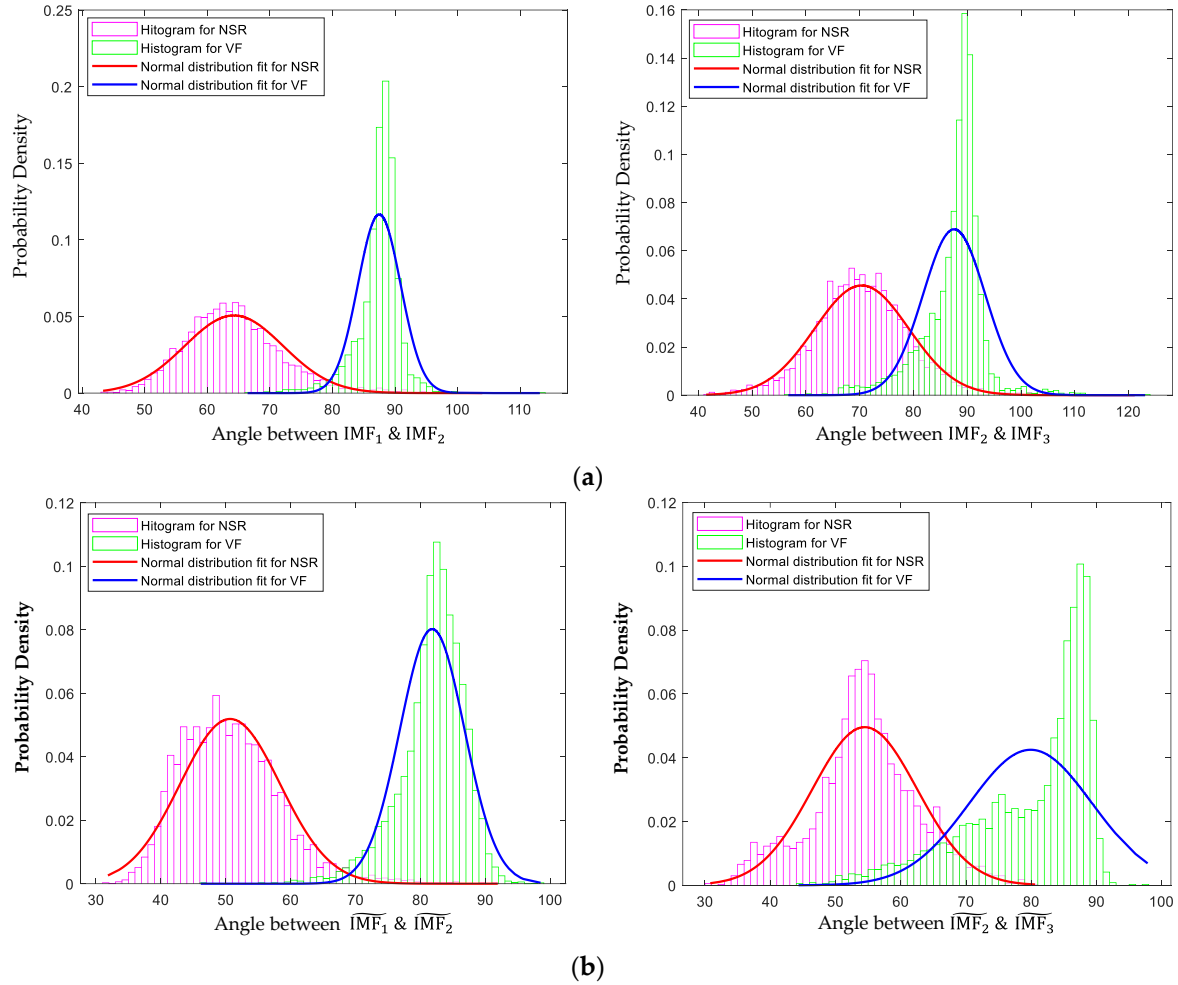

Figure 5. The histogram of the probability distribution for each θ_{12}, θ_{23} between the IMF_1, IMF_2, and IMF_3 of NSR and VF: (**a**) result of EMD from all of the ECG episodes; (**b**) result of EEMD from all of the ECG episodes.

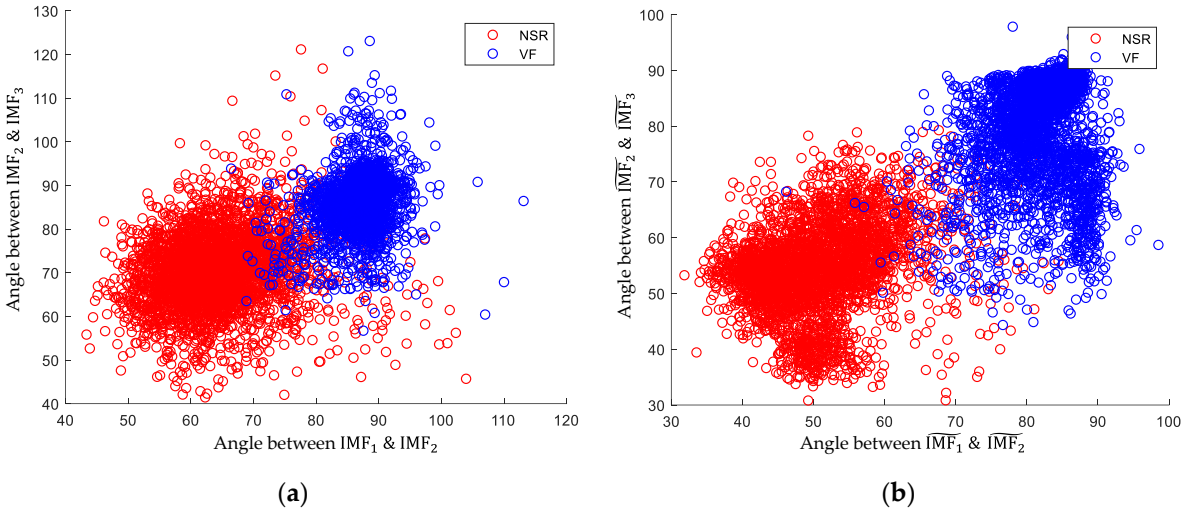

Figure 6. The scatter plots using θ_{12} (the degree between IMF_1 and IMF_2) and θ_{23} (the degree between IMF_2 and IMF_3 of NSR and VF as features: (**a**) scatter plot for θ_{12} and θ_{23} resulting from EMD on all of the ECG episodes; (**b**) scatter plot for θ_{12} and θ_{23} resulting from EEMD on all of the ECG episodes.

Figure 6b illustrates the scatter plot obtained from EEMD for the same angles between IMFs. The distribution of points for NSR (in red) and VF (in blue) shows a pattern similar to that of EMD, where NSR episodes cluster in a different region of the plot compared to VF episodes, albeit with a greater degree of discrimination between the two conditions than in the EMD scatter plot.

The results in Figure 6 suggest that the angles between IMFs, which may indicate the regularity of cardiac rhythms, can serve as distinguishable features to classify ECG signals into NSR and VF. There is a clear distinction between the two states in the scatter plot by EEMD and the less distinct but still observable separation in the scatter plot by EMD.

Table 1 presents the range of θ_{12} and θ_{23} obtained by EMD and EEMD for NSR and VF ECG signals. Table 1 shows the more elaborate ranges, which are not clear in Figures 5 and 6. As can be seen, the angle ranges for VF are generally narrower than for NSR, which is consistent with the visual results in Figures 5 and 6. Furthermore, the differentiation of VF from NSR might be more evident when using EEMD than when using EMD.

Table 1. Range of θ_{12} and θ_{23} obtained by EMD and EEMD for NSR and VF episodes.

Method	ECG Type	Range	
		θ_{12} (Degree)	θ_{23} (Degree)
EMD	NSR	46.2–81.8	50.2–90.3
	VF	78.1–95.2	75.8–98.2
EEMD	NSR	35.2–68.3	36.7–72.6
	VF	71.8–91.7	59.1–90.9

Next, to validate the effectiveness of the proposed features, i.e., θ_{12}, and θ_{23} for discriminating VF and NSR ECG episodes, we used an SVM with a linear kernel classifier. We used a feature vector $\boldsymbol{\theta} = [\theta_{12}\theta_{23}]$ for the input to the SVM classifier. The accuracy was calculated and averaged using 2000 episodes.

Table 2 shows the comparative results of various VF detection algorithms, evaluated based on their sensitivity (Sns.), specificity (Spc.), and overall accuracy, respectively. We carried out 10-fold cross validation. The dataset was randomly divided into ten parts. Nine parts were used as the training set, while one part was used as the test set.

Table 2. Performance comparison between the existing VF detection method and the proposed method. Sensitivity (Sns.), specificity (Spc.), and overall accuracy are presented. For the EMD and EEMD-based methods, the performance is shown as the average ± standard deviation.

Method	Window Length (s)	[1] Sns. (%)	[2] Spc. (%)	Accuracy (%)
Standard exponential [43]	8	50.11	81.70	79.02
Modified exponential [43]	8	51.20	84.11	81.30
Threshold crossing interval [44]	3	82.50	78.10	78.10
Complexity measure [45]	3	97.65	97.48	97.55
Spectral method [46]	6	98.81	69.96	97.87
Hybrid deep learning [47]	3	98.24	95.68	98.53
Fuzzy ClustNet [48]	3	98.92	93.88	98.66
EMD and SVM	3	97.89 ± 1.40	97.68 ± 2.02	97.92 ± 1.52
EEMD and LDA	3	98.03 ± 0.21	97.96 ± 0.32	98.01 ± 0.25

Table 2. *Cont.*

Method	Window Length (s)	[1] Sns. (%)	[2] Spc. (%)	Accuracy (%)
EEMD and RF	3	98.14 ± 0.12	98.69 ± 0.18	98.75 ± 0.11
EEMD and SVM	3	99.22 ± 0.09	99.37 ± 0.15	99.28 ± 0.08

[1] Sensitivity (Sns.), [2] Specificity (Spc.).

The standard exponential algorithm with a window of 8 s achieved a sensitivity of 50.1%, a specificity of 81.7%, and an accuracy of 79%. A slight enhancement in performance is observed using the modified exponential algorithm with the same 8 s window, which improved sensitivity to 51.2%, specificity to 84.1%, and accuracy to 81.3%. The threshold-crossing interval method performed with a sensitivity of 97.70%, a specificity of 97.63%, and an accuracy of 97.65% using a 3 s window, which shows the potential for timely VF detection. The complexity measure recorded a performance comparable to the previous one, with a sensitivity of 97.65%, a specificity of 97.48%, and an accuracy of 97.55% using a 3 s window. The spectral method, which was analyzed over a 6 s window, exhibited a sensitivity of 98.81%, a specificity of 69.96%, and an accuracy of 97.87%. This method's high sensitivity indicates its effectiveness in identifying VF events but also suggests a propensity for false positives, as reflected in the low specificity. The hybrid deep-learning method using a 3 s window achieved a sensitivity of 98.24%, a specificity of 95.68%, and an accuracy of 98.53%. The recently developed Fuzzy ClustNet has a sensitivity of 98.92%, a specificity of 93.88%, and an accuracy of 98.66% with a 3 s window.

For EMD and EEMD-based methods, two features, i.e., θ_{12} and θ_{23}, were used. Using the EMD method with a 3 s window resulted in a noticeable improvement in VF detection, which recorded a sensitivity of 97.89%, a specificity of 97.68%, and an accuracy of 97.92%.

In order to assess the reliance on classifiers that utilize the orthogonality features of EEMD, evaluations of their performance are conducted utilizing a linear discriminant analysis (LDA) [49], random forest (RF) [50], and SVM with a linear kernel. Combining the EEMD method using a 3 s window and LDA produces a sensitivity of 98.03%, a specificity of 97.96%, and an accuracy of 98.01%. In addition, using EEMD with a 3 s window and RF leads to a sensitivity of 98.14%, a specificity of 98.69%, and an accuracy of 98.75%.

The proposed method utilizing EEMD and SVM led to a superior performance compared to its predecessors and EEMD with other classifiers. It performed with a sensitivity of 99.22%, a specificity of 99.37%, and an accuracy of 99.28% using a 3 s window. Moreover, the standard deviations in cases when EEMD is used are less than the standard deviations with EMD in terms of sensitivity, specificity, and overall accuracy.

4. Discussion

4.1. Improvement of VF Detection with Orthogonality Features through EEMD

This work presents an efficient method for detecting ECGs associated with VF using EEMD. The used features, i.e., the angles between the first three IMFS, are chosen based on the observation using the EEMD results of VF and NSR ECG recordings. Thus, this work is motivated by the distinct orthogonality characteristics of low-order IMFs of VF and normal ECGs.

In Figures 5 and 6, we observe that the ranges of θ_{12} and θ_{23} from the EMD and EEMD of NSR and VF are distinct, which is confirmed in Table 1. It is worth noting that the angles θ_{12} and θ_{23} of NSR using EEMD are lower than those using EMD.

In Table 2, we can observe that the VF detection performance of the proposed method is better than previous feature-extraction methods by approximately 49~0.4% in sensitivity, 30~2% in specificity, and 21~1% in accuracy. Compared to these previous methods, the proposed method has achieved a higher sensitivity, specificity, and overall accuracy with short-term ECG recording.

Compared with the deep-learning methods, the proposed method improves VF detection performance by approximately 1~0.3% in sensitivity, 5~3% in specificity, and less than 1% in accuracy.

The recent review work [25] reported that the recent capable deep-learning-based works perform 71~100% in sensitivity, 90.12~99.57% in specificity, and 96~99.53% in accuracy. It suggests that the proposed method performs better than or is comparable to the state of the art. The comparison with deep-learning-based models shows the effectiveness of the proposed orthogonality features [51,52].

In, addition, inspired by the advantage of multiscale features, it is worth substituting the data-driven multiscale analysis, such as the variational mode decomposition (VMD) [53] and empirical wavelet transform (EWT) [54] with EEMD for enhanced VF detection. The detection of fatal VF using short ECG signals is essential for real medical applications, but many studies have not exploited the signal length issue [46,47]. This work has shown the effectiveness of EEMD-based orthogonal features for VF detection, suggesting a useful feature for this issue.

4.2. Limitations

Although the proposed method improved VF discrimination performance, there are still limitations. First, a recent study [55] has shown that EEMD has a reconstruction error due to the use of noise. The elaborated exploitation for applying EEMD and improved data-driven decomposition still needs to be carried out, which includes the robustness of IMFs under varying conditions. At the same time, due to the emphasis on real-time applications, minimizing the computational cost will be of the utmost importance. Second, to be useful in practical medical applications, the proposed method lacks exploration for generalized VF detection for unacquainted samples in practical application. In order to increase the generalization capability, across-database protocols and feature-learning methods need to be developed.

5. Conclusions

In this work, we have presented a new approach to identifying abnormal VF patterns in ECG signals by exploiting the characteristic distinct ECG complex. For this, we use the data-driven EEMD, followed by a measurement of the orthogonality between the first three IMFs. The distinct orthogonality between the IMFs of VF and NSR ECGs by EEMD can serve as simple and efficient features for identifying VF ECGs. By utilizing the improved IMFs extraction of the EEMD technique for short-term ECG signals, the proposed method can achieve a better performance in detecting abnormal VF ECG patterns than other VF detection methods. Thus, the proposed method can address the critical need for rapid and accurate diagnosis of life-threatening VF.

Although our results are promising, we recognize that more investigation is necessary to refine the IMF extraction procedure and verify the suitability of our approach in various datasets and in various clinical contexts. Furthermore, investigating the possibility of incorporating this method into real-time monitoring systems may significantly enhance patient care, particularly for individuals at a high risk of cardiac arrhythmias.

Author Contributions: S.O. and Y.-S.C. conceived and designed the methodology. All authors were responsible for analyzing and writing the paper. All authors have read and agreed to the published version of the manuscript.

Funding: This work was partly supported by the National Research Foundation of Korea (NRF) grant funded by the Korea government (MSIT) (No. NRF-2022R1F1A1075043), the MSIT (Ministry of Science and ICT), Korea, under the ITRC (Information Technology Research Center) support program (IITP-2024-RS-2022-00156225) supervised by the IITP (Institute for Information and Communications Technology Planning, and Evaluation), and the Research Grant of Kwangwoon University in 2022.

Data Availability Statement: Data are contained within the article.

Conflicts of Interest: The authors declare no conflicts of interest.

References

1. Valenza, G.; Faes, L.; Toschi, N.; Barbieri, R. Advanced Computation in Cardiovascular Physiology: New Challenges and Opportunities. *Philos. Trans. R. Soc. A* **2021**, *379*, 20200265. [CrossRef]
2. Kaplan Berkaya, S.; Uysal, A.K.; Sora Gunal, E.; Ergin, S.; Gunal, S.; Gulmezoglu, M.B. A Survey on ECG Analysis. *Biomed. Signal Process. Control* **2018**, *43*, 216–235. [CrossRef]
3. Agrafioti, F.; Hatzinakos, D.; Anderson, A.K. ECG Pattern Analysis for Emotion Detection. *IEEE Trans. Affect. Comput.* **2012**, *3*, 102–115. [CrossRef]
4. Wachowiak, M.P.; Hay, D.C.; Johnson, M.J. Assessing Heart Rate Variability through Wavelet-Based Statistical Measures. *Comput. Biol. Med.* **2016**, *77*, 222–230. [CrossRef] [PubMed]
5. Hammad, M.; Kandala, R.N.V.P.S.; Abdelatey, A.; Abdar, M.; Zomorodi-Moghadam, M.; Tan, R.S.; Acharya, U.R.; Pławiak, J.; Tadeusiewicz, R.; Makarenkov, V.; et al. Automated Detection of Shockable ECG Signals: A Review. *Inf. Sci.* **2021**, *571*, 580–604. [CrossRef]
6. Orini, M.; Pueyo, E.; Laguna, P.; Bailon, R. A Time-Varying Nonparametric Methodology for Assessing Changes in QT Variability Unrelated to Heart Rate Variability. *IEEE Trans. Biomed. Eng.* **2018**, *65*, 1443–1451. [CrossRef]
7. Srinivasan, N.T.; Schilling, R.J. Sudden Cardiac Death and Arrhythmias. *Arrhythm. Electrophysiol. Rev.* **2018**, *7*, 111–117. [CrossRef]
8. Tsao, C.W.; Aday, A.W.; Almarzooq, Z.I.; Alonso, A.; Beaton, A.Z.; Bittencourt, M.S.; Boehme, A.K.; Buxton, A.E.; Carson, A.P.; Commodore-Mensah, Y.; et al. Heart Disease and Stroke Statistics—2022 Update: A Report From the American Heart Association. *Circulation* **2022**, *145*, e153–e639. [CrossRef]
9. Afonso, V.X.; Tompkins, W.J. Detecting Ventricular Fibrillation. *IEEE Eng. Med. Biol. Mag.* **1995**, *14*, 152–159. [CrossRef]
10. Naccarelli, G.V. Electrocardiography of Arrhythmias: A Comprehensive Review. *Circulation* **2012**, *126*, e198. [CrossRef]
11. Mirowski, M.; Mower, M.M.; Reid, P.R. The Automatic Implantable Defibrillator. *Am. Heart J.* **1980**, *100*, 1089–1092. [CrossRef]
12. Benitez, D.; Gaydecki, P.A.; Zaidi, A.; Fitzpatrick, A.P. The Use of the Hilbert Transform in ECG Signal Analysis. *Comput. Biol. Med.* **2001**, *31*, 399–406. [CrossRef]
13. Lee, S.-H.; Chung, K.-Y.; Lim, J.S. Detection of Ventricular Fibrillation Using Hilbert Transforms, Phase-Space Reconstruction, and Time-Domain Analysis. *Pers. Ubiquit Comput.* **2014**, *18*, 1315–1324. [CrossRef]
14. Minami, K.; Nakajima, H.; Toyoshima, T. Real-Time Discrimination of Ventricular Tachyarrhythmia with Fourier-Transform Neural Network. *IEEE Trans. Biomed. Eng.* **1999**, *46*, 179–185. [CrossRef] [PubMed]
15. Nowak, C.-N.; Fischer, G.; Neurauter, A.; Wieser, L.; Strohmenger, H.U. Prediction of Countershock Success: A Comparison of Autoregressive and Fast Fourier Transformed Spectral Estimators. *Methods Inf. Med.* **2009**, *48*, 486–492. [CrossRef] [PubMed]
16. Afonso, V.X.; Tompkins, W.J.; Nguyen, T.Q.; Luo, S. ECG Beat Detection Using Filter Banks. *IEEE Trans. Biomed. Eng.* **1999**, *46*, 192–202. [CrossRef] [PubMed]
17. Khazaee, A.; Ebrahimzadeh, A. Classification of Electrocardiogram Signals with Support Vector Machines and Genetic Algorithms Using Power Spectral Features. *Biomed. Signal Process. Control* **2010**, *5*, 252–263. [CrossRef]
18. Hussein, A.F.; Hashim, S.J.; Aziz, A.F.A.; Rokhani, F.Z.; Adnan, W.A.W. Performance Evaluation of Time-Frequency Distributions for ECG Signal Analysis. *J. Med. Syst.* **2017**, *42*, 15. [CrossRef] [PubMed]
19. Zyout, A.; Alquran, H.; Mustafa, W.A.; Alqudah, A.M. Advanced Time-Frequency Methods for ECG Waves Recognition. *Diagnostics* **2023**, *13*, 308. [CrossRef] [PubMed]
20. Al-Fahoum, A.S.; Howitt, I. Combined Wavelet Transformation and Radial Basis Neural Networks for Classifying Life-Threatening Cardiac Arrhythmias. *Med. Biol. Eng. Comput.* **1999**, *37*, 566–573. [CrossRef]
21. Yodogawa, K.; Ohara, T.; Murata, H.; Iwasaki, Y.; Seino, Y.; Shimizu, W. Detection of Arrhythmogenic Substrate within QRS Complex in Patients with Cardiac Sarcoidosis Using Wavelet-Transformed ECG. *Heart Vessel.* **2020**, *35*, 1148–1153. [CrossRef]
22. Jang, S.-W.; Lee, S.-H. Detection of Ventricular Fibrillation Using Wavelet Transform and Phase Space Reconstruction from Ecg Signals. *J. Mech. Med. Biol.* **2021**, *21*, 2140036. [CrossRef]
23. Praveena, H.D.; Sudha, K.; Geetha, P.; Venkatanaresh, M. Comprehensive Time-Frequency Analysis of Noisy ECG Signals—A Review. *Cardiometry* **2022**, *24*, 271–276. [CrossRef]
24. Xiao, Q.; Lee, K.; Mokhtar, S.A.; Ismail, I.; Pauzi, A.L.B.M.; Zhang, Q.; Lim, P.Y. Deep Learning-Based ECG Arrhythmia Classification: A Systematic Review. *Appl. Sci.* **2023**, *13*, 4964. [CrossRef]
25. Ansari, Y.; Mourad, O.; Qaraqe, K.; Serpedin, E. Deep Learning for ECG Arrhythmia Detection and Classification: An Overview of Progress for Period 2017–2023. *Front. Physiol.* **2023**, *14*, 1246746. [CrossRef]
26. Huang, N.E.; Shen, Z.; Long, S.R.; Wu, M.C.; Shih, H.H.; Zheng, Q.; Yen, N.-C.; Tung, C.C.; Liu, H.H. The Empirical Mode Decomposition and the Hilbert Spectrum for Nonlinear and Non-Stationary Time Series Analysis. *Proc. R. Soc. Lond. Ser. A Math. Phys. Eng. Sci.* **1998**, *454*, 903–995. [CrossRef]
27. Cossul, S.; Andreis, F.R.; Favretto, M.A.; Marques, J.L.B. The Use of Empirical Mode Decomposition on Heart Rate Variability Signals to Assess Autonomic Neuropathy Progression in Type 2 Diabetes. *Appl. Sci.* **2023**, *13*, 7824. [CrossRef]
28. Centeno-Bautista, M.A.; Rangel-Rodriguez, A.H.; Perez-Sanchez, A.V.; Amezquita-Sanchez, J.P.; Granados-Lieberman, D.; Valtierra-Rodriguez, M. Electrocardiogram Analysis by Means of Empirical Mode Decomposition-Based Methods and Convolutional Neural Networks for Sudden Cardiac Death Detection. *Appl. Sci.* **2023**, *13*, 3569. [CrossRef]
29. Khare, S.K.; Gadre, V.M.; Acharya, U.R. ECGPsychNet: An Optimized Hybrid Ensemble Model for Automatic Detection of Psychiatric Disorders Using ECG Signals. *Physiol. Meas.* **2023**, *44*, 115004. [CrossRef] [PubMed]

30. Anas, E.M.A.; Lee, S.Y.; Hasan, M.K. Exploiting Correlation of ECG with Certain EMD Functions for Discrimination of Ventricular Fibrillation. *Comput. Biol. Med.* **2011**, *41*, 110–114. [CrossRef] [PubMed]
31. Wu, Z.; Huang, N.E. Ensemble Empirical Mode Decomposition: A Noise-Assisted Data Analysis Method. *Adv. Adapt. Data Anal.* **2009**, *1*, 1–41. [CrossRef]
32. Chang, K.-M.; Liu, S.-H. Gaussian Noise Filtering from ECG by Wiener Filter and Ensemble Empirical Mode Decomposition. *J. Sign Process Syst.* **2011**, *64*, 249–264. [CrossRef]
33. Hassan, A.R.; Bhuiyan, M.I.H. Automated Identification of Sleep States from EEG Signals by Means of Ensemble Empirical Mode Decomposition and Random under Sampling Boosting. *Comput. Methods Programs Biomed.* **2017**, *140*, 201–210. [CrossRef] [PubMed]
34. Chen, H.; Zhao, C.; Yin, J. Design and Implementation of EEMD-Assisted ICA Joint Denoising Scheme for ECG Signals. *IOP Conf. Ser. Mater. Sci. Eng.* **2019**, *569*, 032059. [CrossRef]
35. Hu, M.; Zhang, S.; Dong, W.; Xu, F.; Liu, H. Adaptive Denoising Algorithm Using Peak Statistics-Based Thresholding and Novel Adaptive Complementary Ensemble Empirical Mode Decomposition. *Inf. Sci.* **2021**, *563*, 269–289. [CrossRef]
36. Yue, Y.; Chen, C.; Wu, X.; Zhou, X. An Effective Electrocardiogram Segments Denoising Method Combined with Ensemble Empirical Mode Decomposition, Empirical Mode Decomposition, and Wavelet Packet. *IET Signal Process.* **2023**, *17*, e12232. [CrossRef]
37. Xia, D.; Meng, Q.; Chen, Y.; Zhang, Z. Classification of Ventricular Tachycardia and Fibrillation Based on the Lempel-Ziv Complexity and EMD. In Proceedings of the 10th International Conference (ICIC 2014), Taiyuan, China, 3–6 August 2014; Huang, D.-S., Han, K., Gromiha, M., Eds.; Springer International Publishing: Cham, Switzerland, 2014; pp. 322–329.
38. Mohanty, M.; Dash, M.; Biswal, P.; Sabut, S. Classification of Ventricular Arrhythmias Using Empirical Mode Decomposition and Machine Learning Algorithms. *Prog. Artif. Intell.* **2021**, *10*, 489–504. [CrossRef]
39. Moody, G.B.; Mark, R.G. The Impact of the MIT-BIH Arrhythmia Database. *IEEE Eng. Med. Biol. Mag.* **2001**, *20*, 45–50. [CrossRef] [PubMed]
40. Blanco-Velasco, M.; Weng, B.; Barner, K.E. ECG Signal Denoising and Baseline Wander Correction Based on the Empirical Mode Decomposition. *Comput. Biol. Med.* **2008**, *38*, 1–13. [CrossRef] [PubMed]
41. Huang, Y.-P.; Li, X.-Y.; Zhang, R.-B. A Research on Local Mean in Empirical Mode Decomposition. In Proceedings of the Computational Science—ICCS, Beijing China, 27–30 May 2007; Shi, Y., van Albada, G.D., Dongarra, J., Sloot, P.M.A., Eds.; Springer: Berlin, Heidelberg, 2007; pp. 125–128.
42. Jia, L.; Zhang, Q.; Zheng, X.; Yao, P.; He, X.; Wei, X. The Empirical Optimal Envelope and Its Application to Local Mean Decomposition. *Digit. Signal Process.* **2019**, *87*, 166–177. [CrossRef]
43. Amann, A.; Tratnig, R.; Unterkofler, K. Reliability of Old and New Ventricular Fibrillation Detection Algorithms for Automated External Defibrillators. *Biomed. Eng. Online* **2005**, *4*, 60. [CrossRef] [PubMed]
44. Thakor, N.V.; Zhu, Y.-S.; Pan, K.-Y. Ventricular Tachycardia and Fibrillation Detection by a Sequential Hypothesis Testing Algorithm. *IEEE Trans. Biomed. Eng.* **1990**, *37*, 837–843. [CrossRef] [PubMed]
45. Zhang, X.S.; Zhu, Y.S.; Thakor, N.V.; Wang, Z.Z. Detecting Ventricular Tachycardia and Fibrillation by Complexity Measure. *IEEE Trans. Biomed. Eng.* **1999**, *46*, 548–555. [CrossRef] [PubMed]
46. Barro, S.; Ruiz, R.; Cabello, D.; Mira, J. Algorithmic Sequential Decision-Making in the Frequency Domain for Life Threatening Ventricular Arrhythmias and Imitative Artefacts: A Diagnostic System. *J. Biomed. Eng.* **1989**, *11*, 320–328. [CrossRef] [PubMed]
47. Sharma, P.; Dinkar, S.K.; Gupta, D.V. A Novel Hybrid Deep Learning Method with Cuckoo Search Algorithm for Classification of Arrhythmia Disease Using ECG Signals. *Neural Comput. Appl.* **2021**, *33*, 13123–13143. [CrossRef]
48. Kumar, S.; Mallik, A.; Kumar, A.; Ser, J.D.; Yang, G. Fuzz-ClustNet: Coupled Fuzzy Clustering and Deep Neural Networks for Arrhythmia Detection from ECG Signals. *Comput. Biol. Med.* **2023**, *153*, 106511. [CrossRef] [PubMed]
49. Martinez, A.M.; Kak, A.C. PCA versus LDA. *IEEE Trans. Pattern Anal. Mach. Intell.* **2001**, *23*, 228–233. [CrossRef]
50. Breiman, L. Random Forests. *Mach. Learn.* **2001**, *45*, 5–32. [CrossRef]
51. Nurmaini, S.; Tondas, A.E.; Darmawahyuni, A.; Rachmatullah, M.N.; Umi Partan, R.; Firdaus, F.; Tutuko, B.; Pratiwi, F.; Juliano, A.H.; Khoirani, R. Robust Detection of Atrial Fibrillation from Short-Term Electrocardiogram Using Convolutional Neural Networks. *Futur. Gener. Comput. Syst.* **2020**, *113*, 304–317. [CrossRef]
52. Plesinger, F.; Andrla, P.; Viscor, I.; Halamek, J.; Jurak, P. Fast Detection of Ventricular Fibrillation and Ventricular Tachycardia in 1-Lead ECG from Three-Second Blocks. In Proceedings of the 2018 Computing in Cardiology Conference (CinC), Maastricht, The Netherlands, 23–26 September 2018; Volume 45, pp. 1–4.
53. Mohanty, M.; Biswal, P.; Sabut, S. Machine Learning Approach to Recognize Ventricular Arrhythmias Using VMD Based Features. *Multidimens. Syst. Sign. Process* **2020**, *31*, 49–71. [CrossRef]

54. Panda, R.; Jain, S.; Tripathy, R.; Acharya, U.R. Detection of Shockable Ventricular Cardiac Arrhythmias from ECG Signals Using FFREWT Filter-Bank and Deep Convolutional Neural Network. *Comput. Biol. Med.* **2020**, *124*, 103939. [CrossRef] [PubMed]
55. Colominas, M.A.; Schlotthauer, G.; Torres, M.E. Improved Complete Ensemble EMD: A Suitable Tool for Biomedical Signal Processing. *Biomed. Signal Process. Control* **2014**, *14*, 19–29. [CrossRef]